Kinetics and continuum emission of negative atomic ions in partially ionized plasmas

W. H. Soon and J. A. Kunc
Department of Aerospace Engineering and Department of Physics, University of Southern California, Los Angeles, California 90089-1191
(Received 10 July 1990)

Kinetics and continuum emission of negative ions are studied in stationary atomic hydrogen, nitrogen, and oxygen plasmas. The intensity of the negative-ion emission was found to be negligible when compared to those of bound-bound and free-bound emission at low and medium particle densities. However, the negative-ion continuum emission can contribute significantly in certain parts of the emission spectrum at high particle densities.

I. INTRODUCTION

Production of continuum radiation in partially ionized electronegative gases has been argued by various authors for some time. An excess of the continuum radiation has been detected in shock and arc experiments,[1-7] but theoretical predictions, neglecting the presence of the negative atomic ions, were not able to explain the differences, especially at electron temperatures $T_e \lesssim 12\,000$ K.[3-5,8] It was suggested[1-4,8] that the excess of the radiation is associated with production of the atomic negative ions by radiative attachment.

In this work, we study a collisional-radiative equilibrium, taking into account negative ions, in atomic hydrogen, atomic nitrogen, and atomic oxygen at electron temperature $T_e = 8000-15\,000$ K and the total particle density $N_t = 10^{10}-10^{18}$ cm^{-3}. We use the stationary nonlinear collisional-radiative models of Refs. 9–11 focusing on production of the negative atomic ions and the associated continuum emission. We refer the reader to Refs. 9–11 for a detailed discussion on the development, assumptions, and solutions presented for that model. Since this paper is based upon the same basic assumptions a brief review is in order.

We consider spatially uniform and electrically neutral plasmas in which the electron-atom (ion) and photon-atom (ion) inelastic collisions dominate thermal nonequilibrium. We assume that the distributions of the translational energies of particles are Maxwellian and that the thermal nonequilibrium is caused by escape of radiation from the plasma. The radiative transport in the gases is treated by using the concept of nonconstant radiative escape factors.[9-11]

II. COLLISIONAL-RADIATIVE EQUILIBRIUM

The steady-state populations of the atomic levels can be determined by balancing all inelastic processes populating and depopulating each level. Similarly, the electron density can be determined by balancing all the processes leading to atomic ionization and recombination. Due to the low N_-/N_e ratio (N_- and N_e are the negative-ion and electron densities, respectively) in the considered plasmas,[10-12] mutual neutralization, reverse mutual neutralization, and the radiative and electron-impact attachments and detachments play a minor role in the production of the electrons and the ground-state and excited atoms. [This can be seen in Figs. 11 and 17 where the populations of the negative ions were calculated from a full system of rate equations.[10,11] This system consisted of the rate equations for production of the negative ions coupled with the rate equations for the production of other species[10,11] (including excited atoms).] Therefore the net production rates for atoms excited to the ith level and for the plasma electrons can be given, respectively, by[13,9]

$$\frac{\partial N_i}{\partial t} = \sum_{k(<i)} N_e N_k C_{ki} + \sum_{j(>i)} N_e N_j R_{ji} + \sum_{j(>i)} N_j A_{ji}\kappa_{ji} + N_e N_+(\alpha_{ci}^R \kappa_{ci} + \alpha_i^D \langle \kappa_{ai} \rangle + N_e \beta_{ci}) - N_i \left[\sum_{j(>i)} N_e C_{ij} + \sum_{k(<i)} N_e R_{ik} + \sum_{k(<i)} A_{ik}\kappa_{ik} + N_e S_{ic} \right], \quad (1)$$

$$\frac{\partial N_e}{\partial t} = \sum_i N_e N_i S_{ic} - \sum_i N_e N_e N_+ \beta_{ci} - \sum_i N_e N_+ (\alpha_{ci}^R \kappa_{ci} + \alpha_i^D \langle \kappa_{ai} \rangle), \quad (2)$$

where N_l is the population of the lth level ($k < i < j$); N_+ is the ground-state positive-ion density; C_{ij} and R_{ji} are rate coefficients for the electron-impact excitation and deexcitation, respectively; A_{ji} is the transition probability (Einstein coefficient) for the $j \rightarrow i$ spontaneous transition; S_{ic} is the electron-impact rate coefficient for ionization of the atom excited to the ith level; α_{ci}^R and β_{ci} are rate coefficients for radiative and three-body recombination, respectively, producing an atom excited to the ith level; α_i^D is the effective dielectronic recombination rate coefficient for the dielectronic transitions to the i "terminating" levels[10,9] (not applicable to hydrogen); and κ_{ji}, κ_{ci}, and $\langle \kappa_{ai} \rangle$ are radiation escape factors for bound-bound, free-bound, and dielectronic radiation, respectively.

The steady-state solutions of Eqs. (1) and (2) coupled

with nonconstant escape factors for given T_e and N_t (the total particle density) can be obtained in the way discussed in Refs. 9–11. The solutions allow one to predict the populations of the plasma atoms and electrons and the intensities of bound-bound, dielectronic, free-bound, free-free, and negative-ion radiation in the plasma. Determination of the negative-ion population is discussed below.

III. NEGATIVE-ION EMISSION

The intensity of the negative-ion emission is given as[12]

$$I_- = \sum_i 4\pi N_e N_i P_i \int \sigma^i_{h\nu,\mathrm{det}}(\nu) \times \exp\left[-\frac{h\nu}{kT_e}\right]\left[\frac{2h\nu^3}{c^2}+J_\nu\right]d\nu - \sum_i 4\pi N_{-,i}\int \sigma^i_{h\nu,\mathrm{det}}(\nu)J_\nu d\nu \ , \tag{3}$$

where the sum is over all the considered ionic levels i and the first term on the right-hand side represents the emission due to radiative attachment and stimulated emissions and the second term represents the absorption due to photodetachment; $\sigma^i_{h\nu;\mathrm{det}}(\nu)$ is the cross section for the photodetachment process which leaves the atom in the ith level, P_i is the Saha equilibrium factor for the negative-ion density defined in Eq. (13), $N_{-,i}$ is the density of the negative ions excited to the ith level, and J_ν is the mean intensity of radiation. Neglecting the stimulated emission and absorption (a good assumption for the negative-ion continuum emission in plasmas considered here[14]), one obtains the emission coefficient, which is expressed in W cm^{-3} sr^{-1} s, for the continuum radiation of the negative ions as

$$j^-_\nu(\nu) = \sum_i 10^{-7} N_e N_i P_i \sigma^i_{h\nu,\mathrm{det}}(\nu)\frac{2h\nu^3}{c^2}\exp\left[-\frac{h\nu}{kT_e}\right] , \tag{4}$$

where the ith level atomic density N_i and the electron density N_e are obtained from Eqs. (1) and (2), respectively. It should be emphasized that the populations of the electrons and the ground-state and excited atoms are controlled by processes other than the processes involving the negative ions. This is because the population of electrons is typically by orders of magnitude greater than population of the negative ions in the plasmas considered here.[10,11] This causes the production of the electrons and the excited atoms to be very weakly dependent on the negative-ion density. As a result, the rate equations for the production of electrons and excited atoms can be decoupled from the rate equations for the production of the negative ions. Therefore knowledge of the population of the negative ions is not needed for determination of the intensity of the continuum radiation produced by the radiative attachment processes.[10–12,7]

Using the approach of Refs. 9–11, we calculated the total plasma continuum emission coefficient $j_\nu = j^{fb}_\nu + j^{ff}_\nu + j^-_\nu$ including the radiation produced by the free-bound (j^{fb}_ν) and free-free (j^{ff}_ν) transitions (involving positive ions) and the radiative attachments (j^-_ν) (involving negative ions) (Figs. 6, 12, and 18).

Summarizing the above, it should be emphasized that Eq. (4) differs from Eq. (5-36) of Ref. 14 (see also its Sec. 5.5), Eq. (15-27) of Ref. 15, and Eq. (63) of Ref. 10. [Even though the expressions of Refs. 14, 15, and 10 look different, they lead in fact to identical results under local thermodynamic equilibrium (LTE) conditions.] In those three expressions, the emission coefficient j^-_ν depends on the density of the negative ions N_- [$N_- = \sum_i N_{-,i}$ and for the ith ionic level $N_{-,i} = N_e N_i P_i K_i$; K_i is a measure of deviation of the ionic population from Saha equilibrium, see Eq. (13)] in the plasma. However, it has been shown in Refs. 10–12, and it can be seen from Eq. (4), that the negative-ion emission coefficient j^-_ν (neglecting stimulated emission and absorption) does not depend on N_- under conditions considered here. Instead, it depends only on N_e, N_i, and T_e; in other words, $K_i = 1$ should be used in all the expressions for j^-_ν given in Refs. 14, 15, and 10. Therefore, in low- and medium-density plasmas, the frequency-dependent coefficients j^-_ν and the corresponding intensity I_- obtained from the expressions of Refs. 14, 15, and 10 would differ from those obtained from Eqs. (4) and (3) of this work. Thus the intensity of the negative-ion continuum radiation given in Figs. 21–23 of Ref. 10 (for atomic oxygen) should be replaced by the corresponding intensities given in Figs. 13–15 of the present work.

IV. PRODUCTION OF NEGATIVE IONS

A. Nitrogen

The production of the unstable $N^-(^3P)$ and metastable $N^-(^1D)$ ions [the density of the $N^-(^1S)$ metastable ions is usually negligible[16]] by radiative attachment can be written as

$$e + N(^4S^\circ) \rightleftarrows N^-(^3P) + h\nu \quad (\gamma_{11},\eta_{11}) \tag{5}$$

and

$$e + N(^2D^\circ) \rightleftarrows N^-(^1D) + h\nu \quad (\gamma_{22},\eta_{22}) \ , \tag{6}$$

where the symbols after the reactions denote the corresponding rate coefficients. [The cross sections for the photodetachments (5) and (6) are taken from Ref. 8.] Then, the radiative attachment cross section can be calculated from the principle of detailed balance.[17]

$$\sigma^i_{h\nu,\mathrm{att}}(\varepsilon) = \frac{g_{-,i}}{g_e g_i}\left[\frac{h\nu}{c}\right]^2 \frac{1}{m_e \varepsilon}\sigma^i_{h\nu,\mathrm{det}}(\nu) \ , \tag{7}$$

where g_e and $g_{-,i}$ (g_i) are statistical weights for the electron and the negative ion (atom) excited to the ith level, respectively, ε is the electron energy, and $h\nu = \varepsilon + U_{-,i}$ ($U_{-,i}$ is the electron affinity for the ith atomic state). The rate coefficients γ_{11} and γ_{22} for the radiative attachments, calculated by integrating the cross sections (7) over the Maxwellian distribution, are given in Fig. 1.

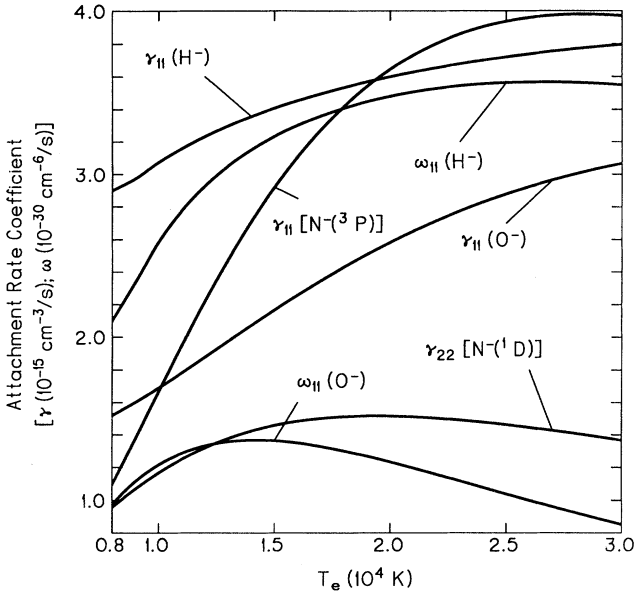

FIG. 1. The radiative attachment rate coefficients: γ_{11} and γ_{22} are rates for the nitrogen atom radiative (two-body) attachment [process (5) and (6), respectively]; γ_{11} is the rate for the oxygen atom radiative (two-body) attachment [process (18)], and ω_{11} is the rate for the electron (three-body) attachment [process (19)]. The rate coefficient γ_{11} for the hydrogen atom is for the radiative (two-body) attachment [process (31)] and the rate coefficient ω_{11} is for the electron (three-body) attachment [process (32)]. The radiative (γ) and three-body (ω) attachment rate coefficients are in 10^{-15} cm^3/s and 10^{-30} cm^6/s, respectively.

We also include in the calculations the contribution of the following processes:

$$e+\mathrm{N}^-(^3P)\rightleftarrows e+\mathrm{N}(^4S^\circ)+e \quad (\mu_{11},\omega_{11}) , \tag{8}$$

$$e+\mathrm{N}^-(^1D)\rightleftarrows e+\mathrm{N}(^2D^\circ)+e \quad (\mu_{22},\omega_{22}) , \tag{9}$$

$$\mathrm{N}^-(^3P,^1D)\rightarrow \mathrm{N}(^4S^\circ)+e \quad (A_{11}^-, A_{21}^-) . \tag{10}$$

The rate coefficients for the three-body attachments (8) and (9) are taken as constants equal to 10^{-30} cm^6/s (neither theoretical nor measured values are available); this is because the three-body attachment rate coefficients ω_{11} for the H$^-$ and O$^-$ ions are weakly dependent on T_e and are approximately 10^{-30} cm^6/s (see Fig. 1). The autodetachment transition probability A_{11}^- is taken to be 10^{14} s^{-1} (Ref. 17). The autodetachment of the N$^-$(^1D) ion is negligible, when compared to the electron-impact detachment (9), because the transition probability for the autodetachment is smaller than 10^5 s^{-1} (Refs. 17–19). It should also mention that inclusion of the processes (8)–(10) in the collisional-radiative model does not influence the production of the ion continuum radiation in plasmas considered here[8] (and see discussion below).

Taking the attachment and detachment processes into account, the balance equations for the production of the N$^-$(^3P) and N$^-$(^1D) ions are, respectively,

$$\frac{\partial N_{-,1}}{\partial t}=N_eN_1(\gamma_{11}+N_e\omega_{11}) -(N_{h\nu}N_{-,1}\eta_{11}+N_eN_{-,1}\mu_{11}+N_{-,1}A_{11}^-) , \tag{11}$$

$$\frac{\partial N_{-,2}}{\partial t}=N_eN_2(\gamma_{22}+N_e\omega_{22}) -(N_{h\nu}N_{-,2}\eta_{22}+N_eN_{-,2}\mu_{22}+N_{-,2}A_{21}^-) , \tag{12}$$

where $N_{-,1}$ and $N_{-,2}$ are the densities for the ground-state [N$^-$(^3P)] and first excited state [N$^-$(^1D)] negative ions, respectively; $N_{h\nu}$ is the photon density and it is assumed that the plasma is transparent to the continuum photons produced in the radiative attachment.

In steady state, the density of the negative ions can be obtained from Eqs. (11) and (12);

$$\frac{N_{-,i}}{N_eN_i}=K_i\left[\frac{g_{-,i}}{g_eg_i}\left[\frac{h^2}{2\pi m_ekT_e}\right]^{3/2}\exp\left[\frac{U_{-,i}}{kT_e}\right]\right] =K_iP_i , \tag{13}$$

where the values of the electron affinities are -0.1 and 0.94 eV for N$^-$(^3P) and N$^-$(^1D), respectively.

Neglecting the small photodetachment terms in Eqs. (11) and (12), the nonequilibrium factors K_i ($i=1,2$) for the populations of the N$^-$(^3P) and N$^-$(^1D) levels are, respectively,

$$K_1=\frac{\gamma_{11}+N_e\omega_{11}}{N_e\omega_{11}+P_1A_{11}^-} \tag{14}$$

and

$$K_2=\frac{\gamma_{22}+N_e\omega_{22}}{N_e\omega_{22}} . \tag{15}$$

B. Oxygen

The photodetachment and electron-impact detachment processes[20,21] are defined, respectively, as

$$h\nu+\mathrm{O}^-(^2P)\rightarrow e+\mathrm{O}(\textstyle\sum(i)) \quad (\eta_{1i}^{\mathrm{tot}}) , \tag{16}$$

$$e+\mathrm{O}^-(^2P)\rightarrow e+\mathrm{O}(\textstyle\sum(i))+e \quad (\mu_{1i}^{\mathrm{tot}}) , \tag{17}$$

where O($\sum(i)$) indicates that the oxygen atom can be in all possible states.

Since the detailed balance relationship relating the *total* cross section for the attachment to the *total* cross section for the detachment is not available, we consider the attachment processes involving only the atomic ground-state O(^3P):

$$e+\mathrm{O}(^3P)\rightarrow \mathrm{O}^-(^2P)+h\nu \quad (\gamma_{11}) , \tag{18}$$

$$e+\mathrm{O}(^3P)+e\rightarrow \mathrm{O}^-(^2P)+e \quad (\omega_{11}) . \tag{19}$$

The cross section for the radiative attachment $\sigma_{h\nu,\mathrm{att}}^1(\varepsilon)$ with the atom in the ground state [process (18)] is calculated by using the principle of detailed balance (7). The

low-energy part ($h\nu \leq 3.5$ eV) of the photodetachment cross section $\sigma^1_{h\nu,\mathrm{det}}(\nu)$ is taken from the experimental measurements of Branscomb[20] while the high-energy part is taken from the theoretical work of Smith.[22] Subsequently, the rate coefficient γ_{11} for radiative attachment to the ground-state atom is calculated by integrating the attachment cross section over the Maxwellian distribution; the rate is very weakly dependent on T_e (see Fig. 1).

The three-body attachment rate coefficient ω_{11} is obtained from the principle of detailed balance as

$$\omega_{11}=\frac{g_{-,1}}{g_e g_1}\left[\frac{h^2}{2\pi m_e kT_e}\right]^{3/2}\exp\left[\frac{U_{-,1}}{kT_e}\right]\mu_{11}=P_1\mu_{11}\ , \tag{20}$$

where μ_{11} is the rate coefficient for the electron-impact detachment to the ground state and it is not available in the literature (the experimental value of $U_{-,1}$ is 1.465 eV). However, under the conditions of this work, μ_{11} is close to the *total* detachment rate coefficient μ^{tot}_{1i}. (This is because the cross sections $\sigma^1_{e,\mathrm{det}}$ and $\sigma^{\mathrm{tot}}_{e,\mathrm{det}}$ are very close to each other up to electron energy of about 4 eV.) The latter rate coefficient is calculated by using the *total* detachment cross section measurement by Tisone and Branscomb.[21] The attachment rate coefficients γ_{11} and ω_{11} and the detachment rate coefficient $\mu^{\mathrm{tot}}_{1i}(\approx\mu_{11})$ are given in Figs. 1 and 2, respectively.

The mutual neutralization and reverse mutual neutralization processes depopulating and populating the negative oxygen ions are

$$\mathrm{O}^-(^2P)+\mathrm{O}^+\rightarrow\mathrm{O}(i)+\mathrm{O}(j)+\Delta E\quad(\alpha_{\mathrm{mut}})\ , \tag{21}$$

$$\mathrm{O}(i)+\mathrm{O}(j)+\Delta E\rightarrow\mathrm{O}^-(^2P)+\mathrm{O}^+\quad(\alpha_{R\,\mathrm{mut}})\ , \tag{22}$$

where we assume that the products of the process (21) are[23] 48% in the $2p^4\,{}^3P(i=1)$ and $2p^3 3p\,{}^3P(j=7)$ states with $\Delta E=1.16$ eV 40% in the $2p^4\,{}^3P(i=1)$ and $2p^3 3p\,{}^5P(j=6)$ states with $\Delta E=1.41$ eV, and 12% in the $2p^4\,{}^1D(i=2)$ and $2p^3 3s\,{}^5S^\circ(j=4)$ states with $\Delta E=1.04$ eV. The rate coefficient for the mutual neutralization, expressed in $\mathrm{cm^3\,s^{-1}}$, was measured by Olson *et al.*,[24] showing, at temperatures from 300 to 3600 K, the following temperature dependence:

$$\alpha_{\mathrm{mut}}=2.8\times10^{-7}\left[\frac{300}{T_{-,+}}\right]^{1/2}\ , \tag{23}$$

where the temperature $T_{-,+}$ (in K) is assumed to be equal to the atomic temperature T_a. It should be added that the rate coefficient given in Eq. (23) (Fig. 2) agrees to within a factor of 2 with the complex potential model calculations of Hickman.[25]

The process (22) can be important at temperatures considered here because ΔE is comparable to the average energy of the particles. The rate coefficient $\alpha_{R\,\mathrm{mut}}$ for the process can be obtained from balancing the process (21) and (22) under collision-dominated, high-density, conditions. Then,

$$\alpha_{R\,\mathrm{mut}}=\frac{N^S_- N^S_+\alpha_{\mathrm{mut}}}{0.48N^S_7N^S_1+0.4N^S_6N^S_1+0.12N^S_4N^S_2}\ , \tag{24}$$

where the populations of the negative ions (N^S_-) and atoms (N^S_i) are calculated from the Saha relationship.

The rate equation for the production of the ground-state $\mathrm{O}^-(^2P)$ ions is

$$\begin{aligned}\frac{\partial N_{-,1}}{\partial t}=&N_eN_1(\gamma_{11}+N_e\omega_{11})\\&+(0.48N_7N_1+0.4N_6N_1+0.12N_4N_2)\alpha_{R\,\mathrm{mut}}\\&-(N_{h\nu}N_{-,1}\eta^{\mathrm{tot}}_{1i}+N_eN_{-,1}\mu^{\mathrm{tot}}_{1i}+N_{-,1}N_+\alpha_{\mathrm{mut}})\ .\end{aligned} \tag{25}$$

Similarly, the steady-state density of the O^- ions can be given, neglecting the small photodetachment term in Eq. (25), by Eq. (13) with the factor K_1:

$$K_1=\frac{\gamma_{11}/N_e+\omega_{11}+(0.48\rho_7G_7+0.4\rho_6G_6+0.12\rho_4G_4B_2F_2)\alpha_{R\,\mathrm{mut}}}{\omega_{11}+P_1\alpha_{\mathrm{mut}}}\ , \tag{26}$$

$$G_i=\frac{g_i}{g_eg_+}\left[\frac{h^2}{2\pi m_ekT_e}\right]^{3/2}\exp\left[\frac{U_i}{kT_e}\right]\ , \tag{27}$$

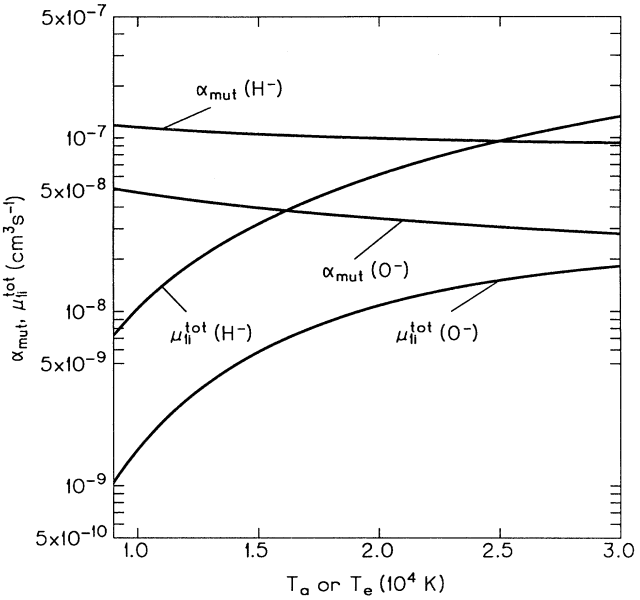

FIG. 2. The total rate coefficients μ^{tot}_{1i} for the electron-impact detachment of the O^- ions [process (17)] and the electron-impact detachment of the H^- ions [process (30)]. The rate coefficients α_{mut} for the mutual neutralization of the O^- and O^+ ions [process (21)] and for the mutual neutralization of the H^- and H^+ ions [process (33)].

where the product B_2F_2 can be approximated by[10]

$$B_2F_2 \approx \frac{g_2}{g_1} \exp\left[-\frac{E_2-E_1}{kT_e}\right], \tag{28}$$

with the nonequilibrium Saha factors $\rho_i = N_i/N_i^S$ defined in Ref. 10 and E_i and U_i being the energy level and ionization potential of the ith atomic level, respectively.

C. Hydrogen

Two processes important for the detachment of the ground-state H^- ions are

$$h\nu + H^- \rightarrow e + H(\textstyle\sum(i)) \quad (\eta_{1i}^{\rm tot}), \tag{29}$$

$$e + H^- \rightarrow e + H(\textstyle\sum(i)) + e \quad (\mu_{1i}^{\rm tot}), \tag{30}$$

where $H(\sum(i))$ indicates that the hydrogen atom can be in all possible states. The *total* cross sections for the photodetachments[26,27] and electron-impact[28–30] detachments are used in the present calculations.

Since the detailed balance relationship relating the *total* cross section for the attachment to the *total* cross section for the detachment is not available, we consider below the attachment processes involving only the atomic ground state,

$$e + H(i=1) \rightarrow H^- + h\nu \quad (\gamma_{11}), \tag{31}$$

$$e + H(i=1) + e \rightarrow H^- + e \quad (\omega_{11}). \tag{32}$$

The cross section for the radiative attachment $\sigma^1_{h\nu,\rm att}(\varepsilon)$ [process (31)] is calculated from the principle of detailed balance (7) using the following photodetachment cross section: $\sigma^1_{h\nu,\rm det}(\nu)$. The low-energy part ($U_{-,1} \le h\nu \le U_{-,1} + E_2$; $U_{-,1}$ is 0.754 eV) of the photodetachment cross section is that of Geltman,[27] while the high-energy part is that of Macek.[26]

The three-body attachment rate coefficient ω_{11} for (32) is obtained by using the detailed balance principle (20) with the electron-impact detachment rate coefficient μ_{11} calculated from the measured detachment cross section of Walton *et al.*[28] (for $U_{-,1} \le \varepsilon \le 25.7$ eV) and of Peart *et al.*[29] (for 25.7 eV $\le \varepsilon \le$ 1000 eV). The attachment rate coefficients γ_{11}, ω_{11} and the detachment rate coefficient $\mu_{1i}^{\rm tot}$ ($\approx \mu_{11}$ in the considered range of temperature) are given in Figs. 1 and 2, respectively.

Another important process depopulating and populating the negative hydrogen ions is the mutual neutralization

$$H^+ + H^- \rightarrow H(i=1) + H(i=3) + \Delta E \quad (\alpha_{\rm mut}), \tag{33}$$

and its reverse process

$$H(i=1) + H(i=3) + \Delta E \rightarrow H^+ + H^- \quad (\alpha_{R\,\rm mut}), \tag{34}$$

where $\Delta E = 0.76$ eV and the products of the process (33) are mainly in the $i=1$ and 3 levels.[23] The cross section for the mutual neutralization, expressed in cm^2, was measured by Moseley *et al.*[31] in an energy range from 0.15 to 300 eV, and the data were fitted below 20 eV to

$$Q_{\rm mut} = \frac{9.18\times10^{-2}}{v^2} + \frac{6.3\times10^{-8}}{v} - 4.5\times10^{-15} + 8.9\times10^{-22} v, \tag{35}$$

where v is the relative speed in cm/s. The mutual neutralization rate coefficient (Fig. 2), expressed in cm^3 s^{-1}, is then calculated by integrating the fitted cross section over the Maxwellian distribution, giving

$$\alpha_{\rm mut} = 9.18\times10^{-2}\left[\frac{2\mu}{\pi k T_{-,+}}\right]^{1/2} + 6.3\times10^{-8} - 4.5\times10^{-15}\left[\frac{8kT_{-,+}}{\mu\pi}\right]^{1/2} + 8.9\times10^{-22}\left[\frac{3kT_{-,+}}{\mu}\right], \tag{36}$$

where μ is the reduced mass of the collision system. The rate coefficient $\alpha_{R\,\rm mut}$ is obtained from balancing the processes (33) and (34) under collision-dominated, high-density conditions,

$$\alpha_{R\,\rm mut} = \frac{N_-^S N_+ \alpha_{\rm mut}}{N_3^S N_1^S}. \tag{37}$$

Balancing the attachment, detachment, and mutual neutralization processes leads to the following equations for production of the ground-state H^- ions:

$$\frac{\partial N_{-,1}}{\partial t} = N_e N_1(\gamma_{11} + N_e\omega_{11}) + N_3 N_1 \alpha_{R\,\rm mut} - (N_{h\nu} N_{-,1}\eta_{1i}^{\rm tot} + N_e N_{-,1}\mu_{1i}^{\rm tot} + N_{-,1}N_+\alpha_{\rm mut}). \tag{38}$$

Neglecting the small photodetachment term in Eq. (38), the steady-state density of the H^- ions can be given by Eq. (13) with

$$K_1 = \frac{\gamma_{11}/N_e + \omega_{11} + (\rho_3 G_3)\alpha_{R\,\rm mut}}{\omega_{11} + P_1\alpha_{\rm mut}}. \tag{39}$$

V. RESULTS AND DISCUSSION

A. Nitrogen

The kinetics of the unstable $N^-(^3P)$ ions is dominated by the autodetachment (10). Therefore the factor K_1 is always below one (its Saha value; Fig. 3). At low and medium densities, the ions are produced mainly by the radiative attachment (5) and, as the electron density increases, by the three-body attachment (8). Therefore, at low and medium densities, the factor K_1 dependence on the gas density is very weak; the number of Eq. (14) is dominated by the N_t-independent rate γ_{11}, while the denominator is dominated by the N_t-independent term $P_1 A_{11}^-$. At higher densities, the $N_e\omega_{11}$ term dominates the γ_{11} term in the numerator of Eq. (14) but it is still much less than the term $P_1 A_{11}^-$. As a result, the factor

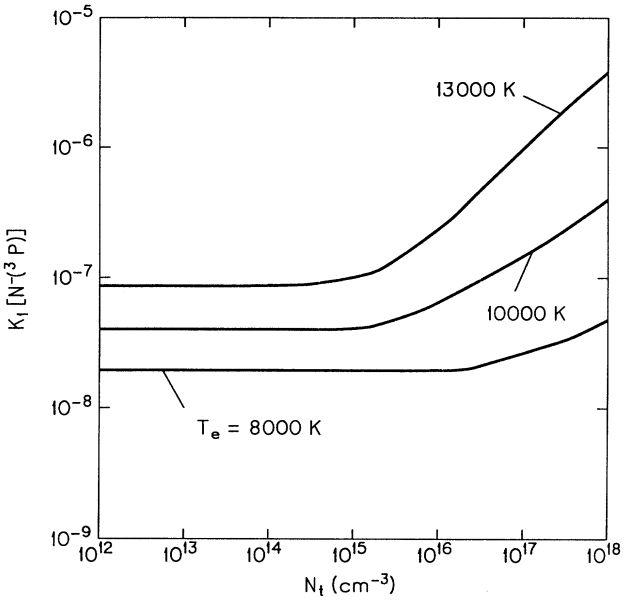

FIG. 3. The population (coefficient K_1) of $N^-(^3P)$ ions in the atomic nitrogen plasma as a function of the total particle density N_t and the electron temperature T_e.

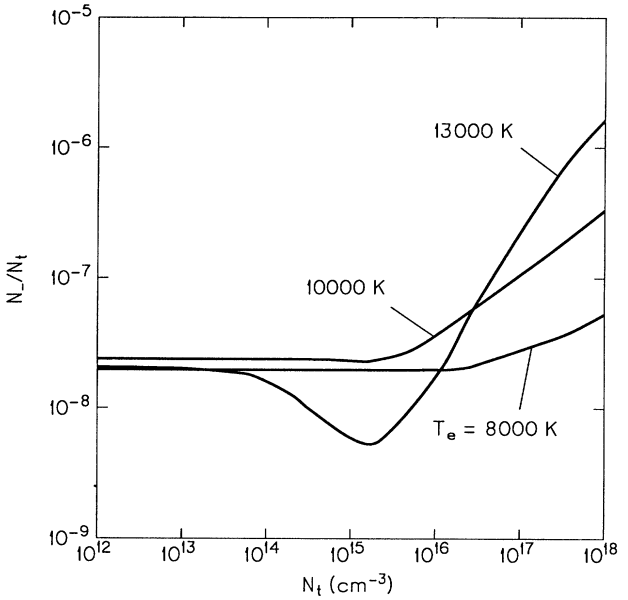

FIG. 5. The ratio of the ion density $N_- = N_{-,1} + N_{-,2}$ to the total particle density N_t as a function of the total particle density N_t and the electron temperature T_e.

K_1 increases with density when $N_t \gtrsim 10^{16}$ cm^{-3}. It should be noted that the factor K_1 is an increasing function of the T_e since the radiative attachment rate γ_{11} increases with T_e while the autodetachment term $P_1 A_{11}^-$ is an inverse function of T_e [see Eq. (14)]. The production of the $N^-(^1D)$ ions is shown in Fig. 4. At the low and medium densities, the production of the negative ions is dominated by the radiative attachment and it is not balanced by the reverse process. Hence the nonequilibrium

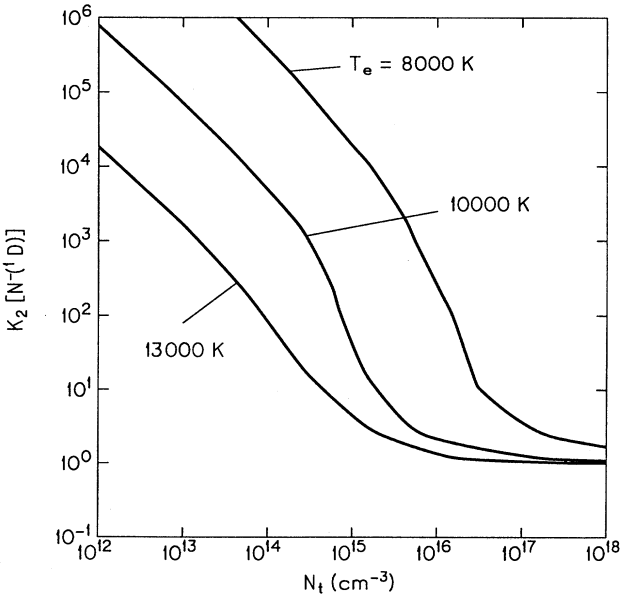

FIG. 4. The population (coefficient K_2) of $N^-(^1D)$ ions in the atomic nitrogen plasma as a function of the total particle density N_t and the electron temperature T_e.

population of the $N^-(^1D)$ ions is higher than its Saha value. As the density increases, the contribution of the three-body attachment becomes more important and it is balanced by the reverse electron-impact detachment; consequently the population of the $N^-(^1D)$ ions approaches the Saha equilibrium. The T_e dependence of the K_2 factor is opposite to that of the K_1 factor. This difference is due to the fact [see Eq. (15)] that both the radiative attachment rate γ_{22} and the three-body attachment rate ω_{22} are weak functions of the electron temperature, while N_e is an increasing function of T_e.

The ratio of N_-/N_t is given in Fig. 5. The total negative-ion density is taken as $N_- = N_{-,1} + N_{-,2}$ and it is dominated by the metastable level $N^-(^1D)$ [the population of the $N^-(^3P)$ level is very low due to the strong autodetachment]. The density of the $N^-(^1D)$ ions is equal to $K_2 P_2 N_2 N_e$. Since $K_2 \sim 1/N_e$, the density of the $N^-(^1D)$ ions is linearly dependent on the density N_2 but weakly dependent on the electron density. At lower temperatures ($T_e \lesssim 10\,000$ K), the ratios N_-/N_t increase with T_e because the density of the $N(^2D^\circ)$ level increases with T_e at all densities.[9] [This is opposite to the behavior of the ratios N_-/N_t in oxygen and hydrogen plasmas, which are decreasing functions of T_e (Figs. 11 and 17 and discussion below).] At $T_e \approx 13\,000$ K (where the nitrogen plasma is close to being fully ionized[9]), the ratio N_-/N_t decreases as N_t increases in the medium-density plasmas ($N_t = 10^{14}$–10^{16} cm^{-3}). This is because depopulation of the $N(^2D^\circ)$ metastable level is then enhanced by the excitation and ionization processes.[9] At higher N_t, the density of the $N(^2D^\circ)$ atoms approaches its Saha value ($\rho_2 = 1$) (Ref. 9) and the ratio N_-/N_t also reaches its Saha value; the T_e dependence of the ratio becomes an increasing function because the population of the $N(^2D^\circ)$ atoms in-

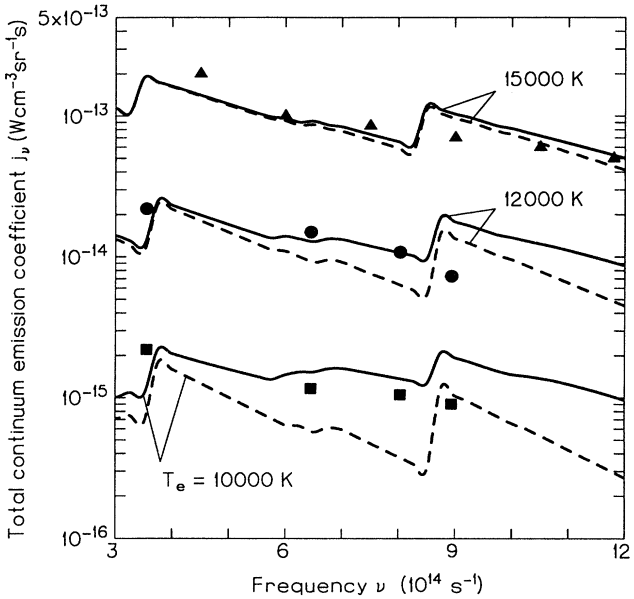

FIG. 6. The comparison of the calculated and measured total continuum emission coefficients j_ν. The solid lines ($j_\nu = j_\nu^{fb} + j_\nu^{ff} + j_\nu^{-}$) represent the result when the contributions of both $N^-(^3P)$ and $N^-(^1D)$ ions are considered, while the dashed lines ($j_\nu = j_\nu^{fb} + j_\nu^{ff}$) represent the results when the contribution of the negative ions is neglected. Experimental results are denoted by squares ($p = 0.61$ atm, $T_e = 10\,000$ K) (Ref. 4), circles ($p = 0.78$ atm, $T_s = 12\,000$ K) (Ref. 4), and triangles ($p = 1$ atm, $T_e = 15\,000$ K) (Ref. 3). The estimated accuracy of the experimental data is better than ±35%.

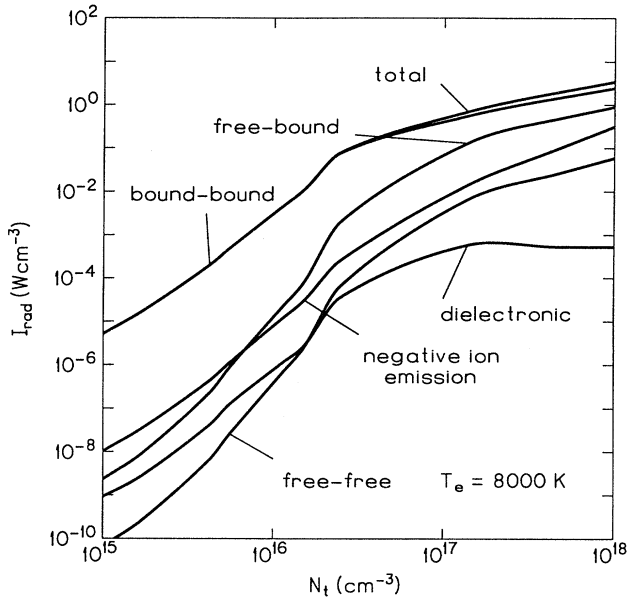

FIG. 7. The intensities of the bound-bound (I_{bb}), dielectronic (I_{di}), free-bound (I_{fb}), free-free (I_{ff}), negative-ion (I_-), and the total (I_{tot}) radiation in the atomic nitrogen plasma. The electron temperature is 8000 K.

creases with T_e at Saha equilibrium.[9]

Comparison of the calculated total emission coefficient $j_\nu = j_\nu^{fb} + j_\nu^{ff} + j_\nu^{-}$ [including contributions of both $N^-(^3P)$ and $N^-(^1D)$ ions and using the theoretical photodetachment cross sections] with its experimental values is shown in Fig. 6. It should be emphasized that the calculated emission coefficients were obtained assuming *theoretical* cross sections for both attachment processes (5) and (6). The choice of the theoretical cross sections over the experimental ones is discussed in detail in Ref. 8. The agreement between the measured and calculated coefficients j_ν is good. Thus it seems that the excess of the continuum radiation detected in the experiments[4,3] can be attributed to the formation of the $N^-(^3P)$ and $N^-(^1D)$ ions through the radiative attachments (5) and (6). As said before $j_\nu^{-} = j_\nu^{-}[N^-(^3P)] + j_\nu^{-}[N^-(^1D)]$, with the first term dominating the continuum emission even though the density of the metastable $N^-(^1D)$ ions is higher than the density of the unstable $N^-(^3P)$ ions. The contribution of the negative-ion emission coefficient to the total continuum emission coefficient can also be seen in Fig. 6. For example, the negative-ion emission contributes from about 72% (when $T_e = 10\,000$ K), 40% (when $T_e = 12\,000$ K) to 10% (when $T_e = 15\,000$ K) of the total emission coefficient at $\nu = 8 \times 10^{14}$ s^{-1} (or $\lambda = 2667$ Å). Thus the contribution of the negative-ion emission to the total continuum emission is certainly not negligible in the nitrogen plasmas considered here. [One should add that no excess of continuum radiation was detected in the existing higher pressure ($p > 30$ atm) and higher electron temperature ($T_e \gtrsim 13\,000$ K) experiment of Cooper.[32] This, however, is expected because of the negligible contributions of the negative-ion emission to the total continuum radiation[10,11,5] in plasmas with high electron temperature.]

Various kinds of radiation produced in atomic nitrogen are shown in Figs. 7–9. At low and medium densities,

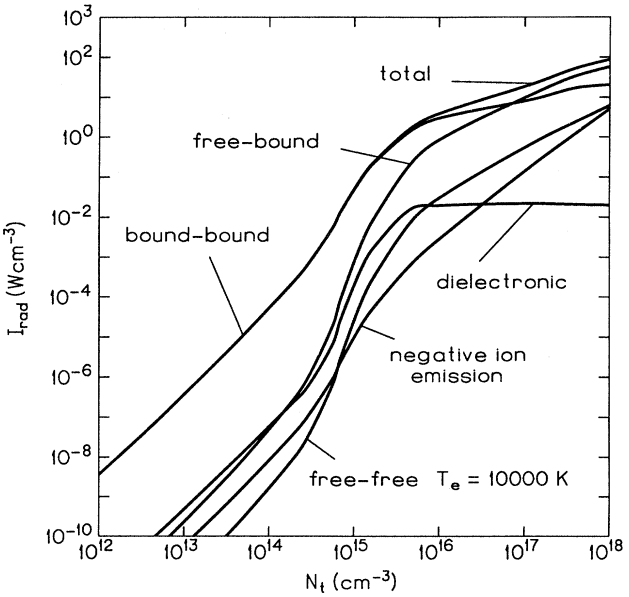

FIG. 8. The intensities of the bound-bound (I_{bb}), dielectronic (I_{di}), free-bound (I_{fb}), free-free (I_{ff}), negative-ion (I_-), and the total (I_{tot}) radiation in the atomic nitrogen plasma. The electron temperature is 10 000 K.

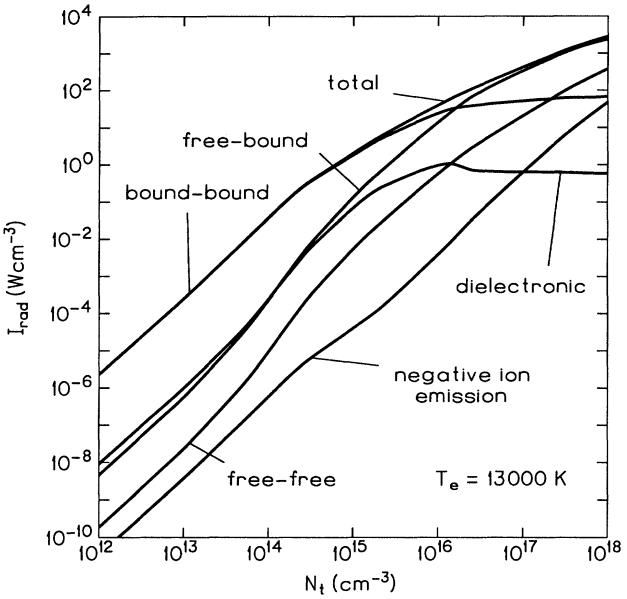

FIG. 9. The intensities of the bound-bound (I_{bb}), dielectronic (I_{di}), free-bound (I_{fb}), free-free (I_{ff}), negative-ion (I_-), and the total (I_{tot}) radiation in the atomic nitrogen plasma. The electron temperature is 13 000 K.

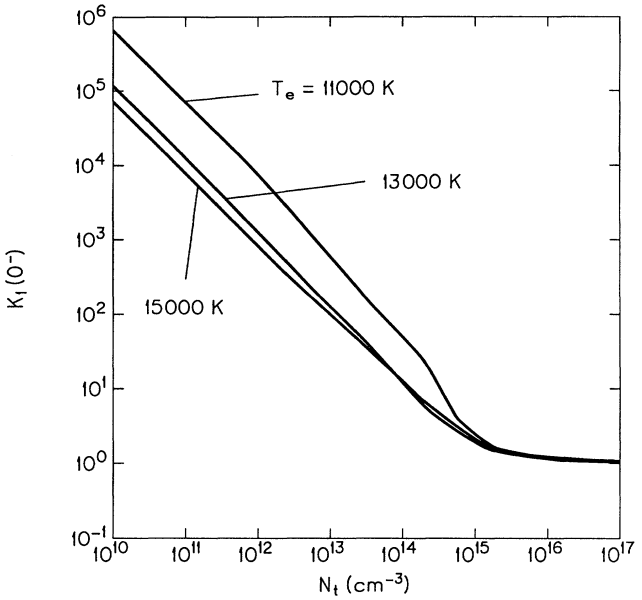

FIG. 10. The population (coefficient K_1) of $O^-(^2P)$ ions in the atomic oxygen plasma as a function of the total particle density N_t and the electron temperature T_e.

the bound-bound radiation dominates the plasma radiation.[9] The intensity of the negative-ion emission is then larger than the other continuum emissions only at lower ($\lesssim$8000 K) temperatures. This is because at these temperatures the plasma ionization degree is small.[9] Consequently, the negative-ion emission through the radiative attachment is much more efficient than the free-bound (through radiative recombination) and free-free (through bremsstrahlung) radiation. At higher densities, the free-bound and free-free radiation become more important when reabsorption of the bound-bound radiation becomes high. The intensity of the negative-ion radiation is comparable to the free-bound and free-free radiation at lower temperatures. (Dielectronic recombination radiation, competing at low densities with the free-bound radiation, is strongly reabsorbed at higher densities and its importance diminishes).

B. Oxygen

At low density N_t, the production of the $O^-(^2P)$ ions is controlled by the radiative attachment. (The reverse mutual neutralization is not effective because the densities of the $i=6,7$ atomic levels are low as a result of the high frequency of their ionization and the radiative decay.) These ions are destroyed by the mutual neutralization (mainly) and the electron-impact detachment. Destruction of the $O^-(^2P)$ ions by photodetachment is not effective because the continuum radiation is poorly reabsorbed.[14] At higher density, the population of the $i=6,7$ atomic levels approaches its equilibrium value and the production of the negative ions is dominated by the reverse mutual neutralization; as a result, the population of the $O^-(^2P)$ ions is controlled by the balance of the mutual neutralization and reverse mutual neutralization.

The production of the $O^-(^2P)$ ions (the factor K_1) is shown in Fig. 10. At low and medium densities, it is higher than its Saha value because it is dominated by the radiative attachment which is not balanced by the reverse process. Also, the factor K_1 is a decreasing function of the electron temperature [see Eq. (26)] because in such a case the factor is controlled by the radiative attachment

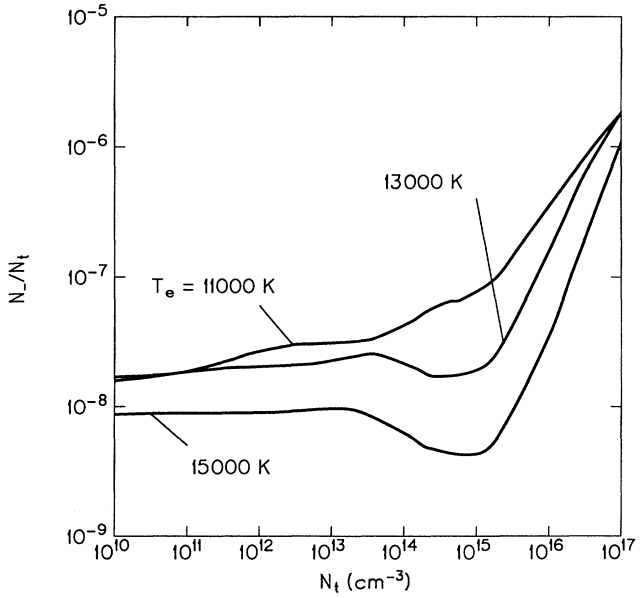

FIG. 11. The ratio of the $O^-(^2P)$ ion density to the total particle density (N_-/N_t) as a function of the particle density N_t and the electron temperature T_e.

term γ_{11}/N_e; γ_{11} is a weak function of T_e, while N_e increases with T_e.[10] As the density N_t increases, the production and destruction of the negative ions are more and more controlled by the mutual neutralization and its reverse process. Finally, at high densities, the negative-ion population reaches Saha equilibrium.

The ratio N_-/N_t ($N_-=N_{-,1}$) is given in Fig. 11. The T_e dependence of the ratio is weaker than the T_e dependence of the ionization degree.[10] This is because the efficiencies of the processes producing and destroying the negative ions are very weak functions of T_e in the entire range of temperatures. The ratios are decreasing functions of T_e since the N_- is proportional to the atomic ground-state density N_1 which is a decreasing function of T_e.[10] For a given T_e, the ratio N_-/N_t is practically independent of N_t at low and medium densities which is a result of a linear dependence of the density N_- on N_t. [The balance between the production and destruction of the $O^-(^2P)$ ions leads to the following relationship:

$$N_- \sim N_t \frac{\gamma_{11}(T_e)}{\alpha_{\text{mut}}(T_{-,+} \approx T_a)} , \tag{40}$$

where both rates are weak functions of temperature (Figs. 1 and 2).] At high N_t, mutual neutralization and reverse mutual neutralization dominate the kinetics of the negative ions causing the ion density to be in Saha equilibrium.

Experimental work on microscopic properties of the high-temperature oxygen is very limited. The only existing data are the frequency-dependent measurements of the continuum radiation produced in high-density oxygen discharge.[6] The comparison of our results with the measured values of the total emission coefficient $j_\nu = j_\nu^{fb} + j_\nu^{ff} + j_\nu^{-}$ is given in Fig. 12. As can be seen from Fig. 12, the agreement between the measurement intensity and the predicted one is good. The present calculations show that the negative-ion emission is important in the frequency range of continuum radiation considered in the comparison ($U_{-,1} \leq h\nu \lesssim 3$ eV). The contribution

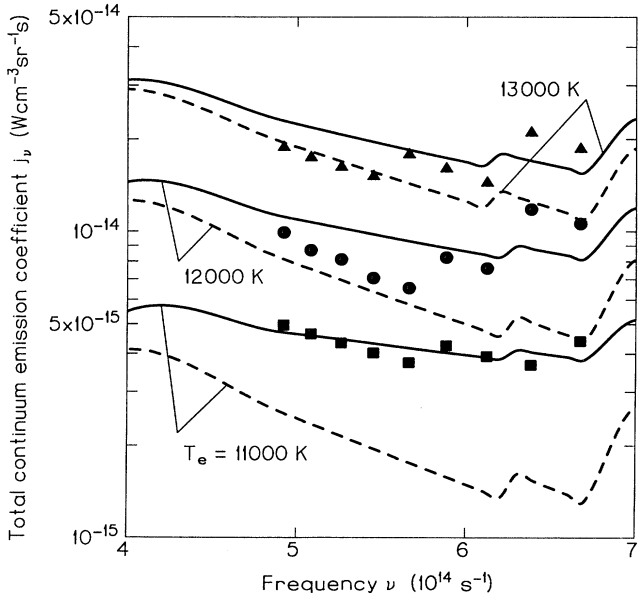

FIG. 12. Comparison of the calculated (solid lines) and measured total continuum emission coefficients $j_\nu = j_\nu^{fb} + j_\nu^{ff} + j_\nu^{-}$ for $T_e = 11\,000$ K (squares), 12 000 K (circles), 13 000 K (triangles) and $P = 1$ atm (Ref. 6). The dashed lines are the calculated continuum emission coefficients ($j_\nu = j_\nu^{fb} + j_\nu^{ff}$) when the negative-ion emission is neglected.

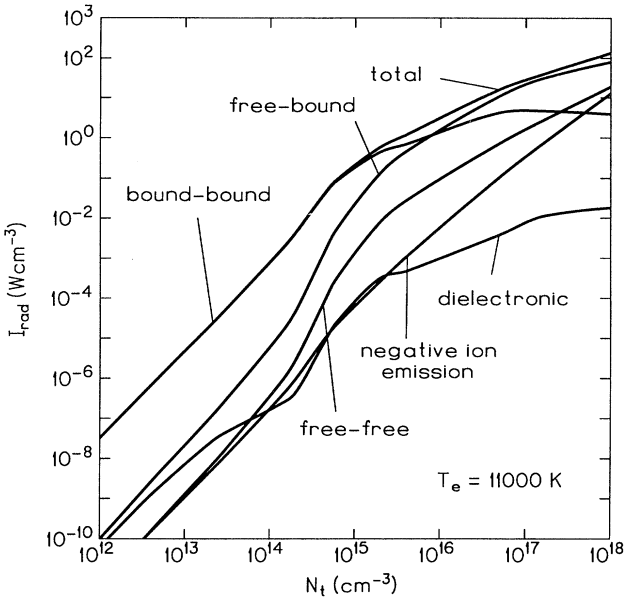

FIG. 13. The intensities of the bound-bound (I_{bb}), dielectronic (I_{di}), free-bound (I_{fb}), free-free (I_{ff}), negative-ion (I_-), and the total (I_{tot}) radiation in the atomic oxygen plasma. The electron temperature is 11 000 K.

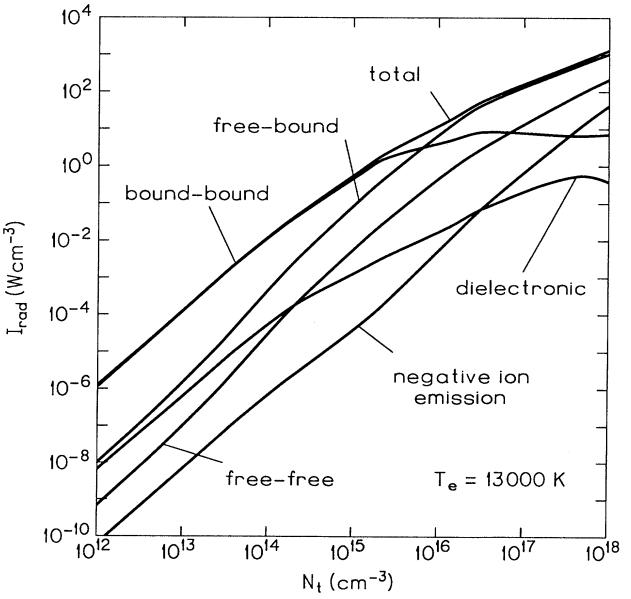

FIG. 14. The intensities of the bound-bound (I_{bb}), dielectronic (I_{di}), free-bound (I_{fb}), free-free (I_{ff}), negative-ion (I_-), and the total (I_{tot}) radiation in the atomic oxygen plasma. The electron temperature is 13 000 K.

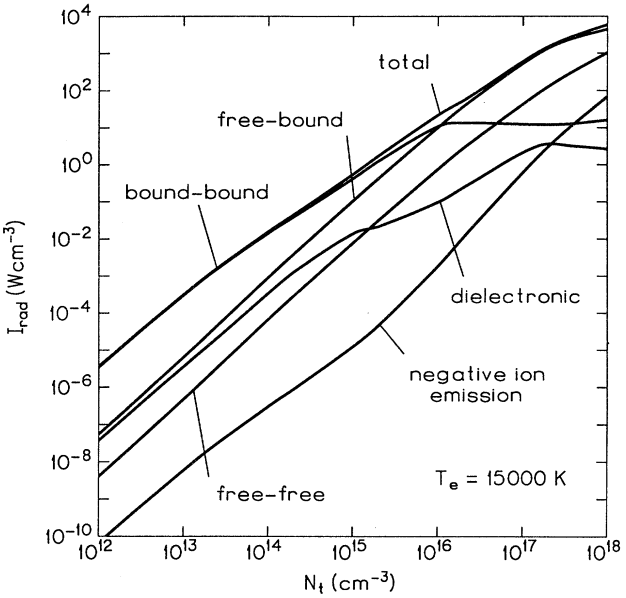

FIG. 15. The intensities of the bound-bound (I_{bb}), dielectronic (I_{di}) free-bound (I_{fb}), free-free (I_{ff}), negative-ion (I_-), and the total (I_{tot}) radiation in the atomic oxygen plasma. The electron temperature is 15 000 K.

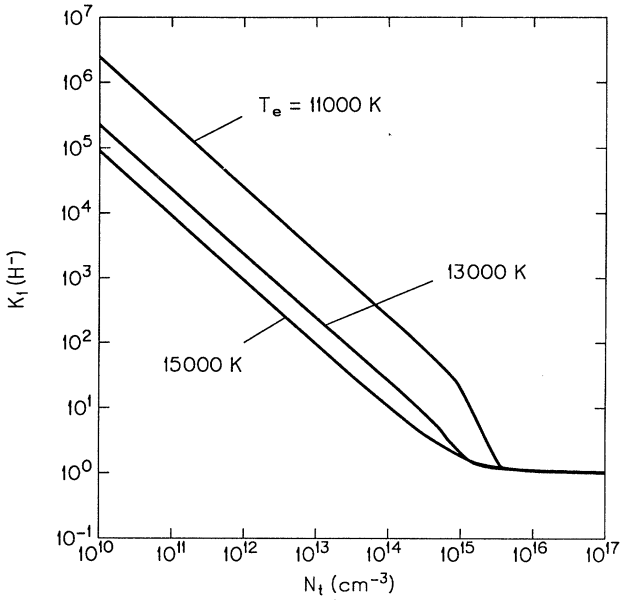

FIG. 16. The population (coefficient K_1) of H^- ions in the atomic hydrogen plasma as a function of the total particle density N_t and the electron temperature T_e.

of the negative-ion emission to the total continuum emission is clearly illustrated in Fig. 12. For example, at $\nu = 6\times10^{14}$ s^{-1} (or $\lambda = 5000$ Å), the negative-ion emission makes about 62% (when $T_e = 11\,000$ K) to 26% (when $T_e = 13\,000$ K) of the total continuum radiation produced by the oxygen plasma. Thus inclusion of the negative-ion continuum emission is necessary for correct interpretation of the mechanisms producing the continuum radiation in the oxygen plasmas.

Various kinds of radiation produced in the atomic oxygen are shown in Figs. 13–15. At low and medium densities, the bound-bound radiation dominates the total plasma radiation. The intensity of the negative-ion emission is considerably smaller than other kinds of continuum radiation. It should be noted that the role of the negative-ion emission is less important in atomic oxygen than in atomic nitrogen. Also, at low density, the dielectric recombination radiation is competing with the free-bound radiation in a way similar to that in atomic nitrogen. At higher densities, the free-bound and free-free radiation become important, and the relative role of the negative-ion radiation also becomes more important (especially at lower temperatures). At these densities, the negative-ion emission is higher than the bound-bound and dielectronic recombination emissions because reabsorption of the two latter emissions is quite high.

C. Hydrogen

The kinetics of the H^- ions in atomic hydrogen do not affect significantly the populations of the electrons, positive ions, and excited atoms because the ratio N_-/N_e is always very small as a result of the very rapid mutual neutralization (Figs. 16 and 17). One should add that the mutual neutralization is much more effective in destroying the H^- ions than in destroying the H^+ ions because the excited ($i = 3$) atoms, the main product of the neutralization, are both strongly radiative and easy to ionize. It must be emphasized that although the production of the H^- ions in the plasma is not as high as the production of electrons, the contribution of the negative-ion

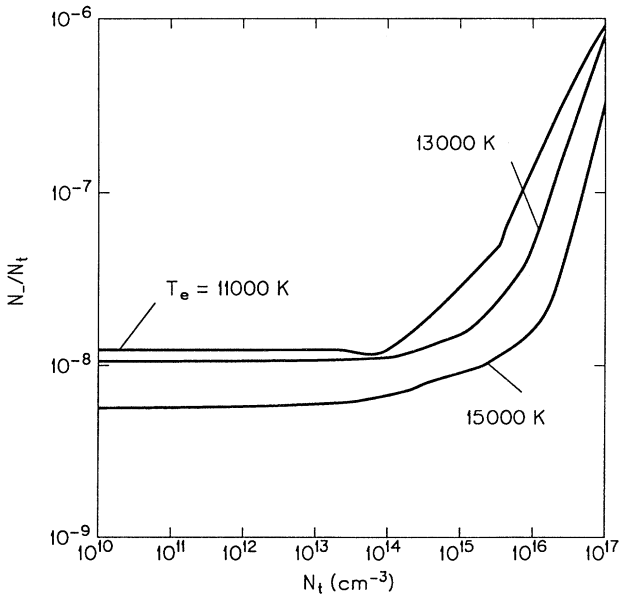

FIG. 17. The ratio of the H^- ion density to the total particle density (N_-/N_t) as a function of the total particle density N_t and the electron temperature T_e.

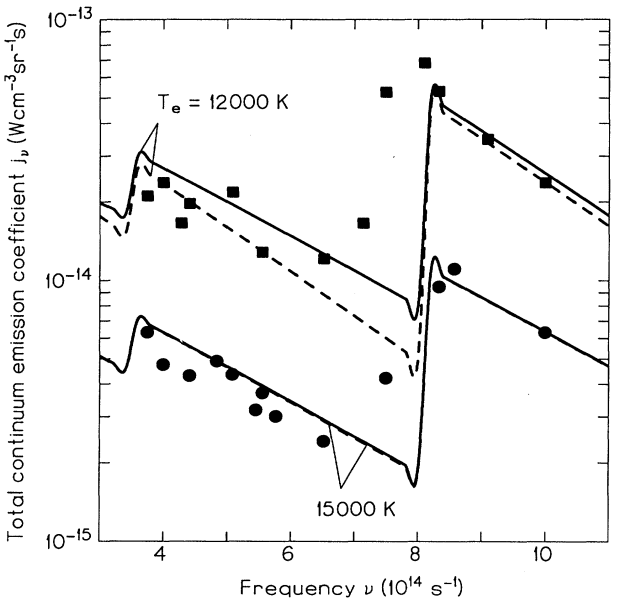

FIG. 18. Comparison of the calculated (solid lines) and measured total continuum emission coefficients $j_\nu = j_\nu^{fb} + j_\nu^{ff} + j_\nu^{-}$ for $T_e = 12\,000$ K, $N_e = 5.8 \times 10^{16}$ cm^{-3} (squares), and 15 000 K, $N_e = 3.1 \times 10^{16}$ cm^{-3} (circles) (Ref. 7). The dashed lines are the calculated continuum emission coefficients ($j_\nu = j_\nu^{fb} + j_\nu^{ff}$) when the negative-ion emission is neglected.

emission (due to the radiative attachment) to the total production of the continuum radiation is certainly not negligible (Fig. 18).

The measurements of the total continuum emission coefficient in the range of the visible and ultraviolet wavelengths by Hamberger and Johnson[7] are compared with our results ($j_\nu = j_\nu^{fb} + j_\nu^{ff} + j_\nu^{-}$) in Fig. 18. As can be seen from Fig. 18, the agreement of the measured coefficient with the predictions of this work is good, except near the wavelength 4000–4200 Å (frequency 7×10^{14}–7.5×10^{14} s^{-1}). At these frequencies, the experimental data most likely include the spectral line emission of the highly broadened Balmer lines that overlap with background continuum emission.[7] The present calculations show that the negative-ion emission can be important in atomic hydrogen plasma. For example, at $\lambda = 5000$ Å (or $\nu = 6 \times 10^{14}$ s^{-1}), the negative-ion emission accounts for about 30% of the total continuum radiation produced by the hydrogen plasma with $T_e = 12\,000$ K. (Detailed discussion of the comparison of the intensities of the negative-ion emission with the bound-bound, free-bound, and free-free radiation is given in Ref. 11.)

VI. SUMMARY

In the atomic gases considered here, the density of negative ions is always several orders of magnitude less than the total gas density, and less than the electron density. Therefore the contribution of the negative ions to production of electrons, positive ions, and excited atoms is negligible when compared with the contribution of other species. The low production of the negative ions is due to several facts. First, the efficiency of production of negative ions is limited by the number of both electrons and atoms available in the plasmas. In addition to this limitation, the efficiencies of the autodetachment and electron-impact detachment are always much higher than the efficiencies of the attachment processes.

The nonequilibrium population of the stable negative ions is always above the corresponding Saha value. This is because the radiative attachment of these ions is not balanced by the reverse photodetachment. The nonequilibrium population of the unstable negative ions is always below its Saha value because of the strong and unbalanced autodetachment.

In general, the total radiative power associated with the negative-ion emission is negligible when compared to other continuum and spectral radiation. However, in a certain range of frequency (10^{14}–10^{15} s^{-1}) the negative-ion continuum emission can contribute significantly (up to 70%) to the total continuum emission. This contribution is especially distinctive at lower plasma temperatures ($\lesssim 12\,000$ K).

ACKNOWLEDGMENTS

This work was supported by the National Aeuronautics and Space Administration, Grant No. NAGW-1061 and the Air Force Office of Scientific Research, Grant Nos. 88-0119 and 88-0146.

[1]G. Boldt, Z. Phys. **154**, 330 (1959).
[2]G. M. Thomas and W. A. Menard, AIAA J. **5**, 2214 (1967).
[3]Z. J. Asinovskii, A. V. Kirillin, and G. A. Kobsev, J. Quant. Spectrosc. Radiat. Transfer **10**, 143 (1970).
[4]D. L. Cliffone and J. G. Borucki, J. Quant. Spectrosc. Radiat. Transfer **11**, 1291 (1971).
[5]L. G. D'Yachkov, O. A. Golubev, G. A. Kobsev, and A. N. Vargin, J. Quant. Spectrosc. Radiat. Transfer **20**, 175 (1978).
[6]G. Boldt, Z. Phys. **154**, 319 (1959).
[7]S. M. Hamberger and A. W. Johnson, J. Quant. Spectrosc. Radiat. Transfer **5**, 683 (1965).
[8]W. H. Soon and J. A. Kunc, Phys. Rev. A **41**, 4531 (1990).
[9]J. A. Kunc and W. H. Soon, Phys. Rev. A **40**, 5822 (1989)
[10]W. H. Soon and J. A. Kunc, Phys. Rev. A **41**, 825 (1990).
[11]W. H. Soon and J. A. Kunc, Phys. Fluids B **2**, 2833 (1990).
[12]J. E. Vernazza, E. H. Avrett, and R. Loeser, Astrophys. J. Suppl. Ser. **45**, 635 (1981).
[13]D. R. Bates, A. E. Kingston, and R. W. P. McWhirter, Proc. R. Soc. London Ser. A **267**, 297 (1962).
[14]H. R. Griem, *Plasma Spectroscopy* (McGraw-Hill, New York, 1964).
[15]H. S. W. Massey, E. S. W. Burhop, and H. B. Gilbody, *Electronic and Ionic Impact Phenomena* (Oxford University Press, London, 1969).

[16]L. G. D'Yachkov, G. A. Kobsev, and G. E. Norman, Zh. Eksp. Teor. Fiz. **65**, 1399 (1973) [Sov. Phys.—JETP **38**, 697 (1974)].
[17]H. S. W. Massey, *Negative Ions* (Cambridge University Press, Cambridge, England, 1976).
[18]H. Hiraoka, R. K. Nesbet, and L. W. Welsh, Jr., Phys. Rev. Lett. **39**, 130 (1977).
[19]B. M. Smirnov, *Negative Ions* (McGraw-Hill, New York, 1982).
[20]L. M. Branscomb, in *Atomic and Molecular Processes,* edited by D. R. Bates (Academic, New York, 1962), p. 100.
[21]G. C. Tisone and L. M. Branscomb, Phys. Rev. **170**, 169 (1968).
[22]S. J. Smith, in *Proceedings of the Fourth International Conference on Ionization Phenomena in Gases, Uppsala, 1959,* edited by N. R. Nilsson (North-Holland, Amsterdam, 1960), p. 219.
[23]R. E. Olson, J. R. Peterson, and J. T. Moseley, J. Geophys. Res. **76**, 2516 (1971).
[24]R. E. Olson, J. R. Peterson, and J. T. Moseley, J. Chem. Phys. **53**, 3391 (1970).
[25]A. P. Hickman, J. Chem. Phys. **70**, 4872 (1979).
[26]J. Macek, Proc. Phys. Soc. London **92**, 365 (1967).
[27]S. Geltman, Astrophys. J. **136**, 935 (1962).
[28]D. S. Walton, B. Peart, and K. T. Dolder, J. Phys. B **4**, 1343 (1971).
[29]B. Peart, D. S. Walton, and K. T. Dolder, J. Phys. B **3**, 1346 (1970).
[30]O. Bely and S. B. Schwartz, J. Phys. B **2**, 159 (1969).
[31]J. T. Moseley, W. H. Aberth, and J. R. Peterson, Phys. Rev. Lett. **24**, 435 (1970).
[32]D. M. Cooper, J. Quant. Spectrosc. Radiat. Transfer **12**, 1175 (1972).